Environmental Science Advances

ROYAL SOCIETY OF CHEMISTRY

PAPER

View Article Online
View Journal | View Issue

Cite this: *Environ. Sci.: Adv.*, 2025, **4**, 1684

Polymer-enhanced nickel ferrite catalyst for the efficient reduction of 4-nitrophenol as a hazard pollutant

Ghizlene Boudghene Stambouli,[ab] Belkacem Benguella,[b] Makhoukhi Benamar[b] and Ayman H. Kamel *[ac]

The synthesized nickel ferrite ($NiFe_2O_4$)/poly(aniline-*co*-*o*-toluidine) (PAOT) nanocomposite was successfully characterized using XRD, FTIR, SEM, and EDX, confirming the formation of a stable spinel structure with uniform particle distribution (32–68 nm). The material exhibited a low bandgap energy of 1.24 eV and retained magnetic properties, enabling easy recovery and reuse for up to four cycles. The catalytic activity of the $NiFe_2O_4$/PAOT nanocomposite was evaluated for the visible-light-assisted reduction of 4-nitrophenol (4-NP) without external reducing agents. The catalyst achieved reduction efficiencies of 85.83% at 2 ppm, 95% at 10 ppm, and 99% at 15 ppm within 60 min, with improved performance at higher catalyst dosages and temperatures (*e.g.*, 50 °C with 20 mg). Kinetic analysis revealed pseudo-first-order behavior. Compared to other reported catalysts, $NiFe_2O_4$/PAOT offers green synthesis, high efficiency, magnetic recoverability, and operational simplicity, making it a promising material for sustainable wastewater treatment.

Received 9th May 2025
Accepted 26th August 2025

DOI: 10.1039/d5va00128e

rsc.li/esadvances

Environmental significance

The presence of 4-nitrophenol (4-NP) in wastewater poses a significant environmental and health hazard due to its toxicity, persistence, and resistance to conventional degradation methods. This study introduces a highly efficient and sustainable approach for 4-NP reduction using $NiFe_2O_4$/POAT nanocomposite catalysts, which demonstrate exceptional catalytic performance under visible light conditions. The low bandgap energy (1.24 eV) enhances electron transfer, enabling effective degradation of pollutants without reliance on UV irradiation, making the process more energy-efficient. Furthermore, the magnetic properties of the catalyst allow for easy recovery and reuse, reducing secondary waste generation and operational costs. With a 95% reduction efficiency within one hour and reusability over multiple cycles, $NiFe_2O_4$/POAT offers a scalable and environmentally friendly alternative for wastewater treatment. These findings contribute to the development of sustainable catalytic systems that align with green chemistry principles, paving the way for improved strategies in water purification and environmental remediation.

Introduction

Globally, the development of new and creative solutions for the effective treatment of wastewater that contains harmful organic contaminants is very important.[1,2] Water is one of the primary components that sustain life on Earth. Every day, water is used for various purposes and is essential to every bodily function. Numerous things contribute to water contamination, such as agriculture, industry, and urbanization. Agricultural and industrial operations result in water contamination from fertilizers, chemicals, pesticides, heavy metals, diseases, *etc.* The health of both humans and animals is now at risk due to such activities.[3]

Aromatic nitrophenols, including 4-nitrophenol, are significant contributors to water pollution due to their extensive use in industries such as pesticides, fertilizers, dyes, paper, and plasticizers production. Additionally, they serve as precursors in the synthesis of paracetamol in the pharmaceutical industry. These nitrophenols are highly toxic, with exposure linked to carcinogenic effects in humans and other living organisms. The World Health Organization (WHO) and the U.S. Environmental Protection Agency (EPA) classify 4-nitrophenol (4-NP) as a highly toxic substance. To safeguard public health, regulations like the Mexican NOM-127-SSA1-19 945 set its permissible concentration in drinking water at 1 μg L^{-1}.[4] Prolonged or high exposure to 4-NP can impair the nervous system and reduce the blood's oxygen-carrying capacity. Inhalation of 4-NP may result in respiratory issues, including throat and lung irritation, coughing, and shortness of breath, along with systemic effects such as nausea, weakness, rapid heart rate, disorientation, and fever.

[a]*Chemistry Department, College of Science, University of Bahrain, Sakhir 32038, Kingdom of Bahrain. E-mail: ahkamel76@sci.asu.edu.eg; amohamed@uob.edu.bh*
[b]*Inorganic Chemistry and Environment Laboratory, University of Tlemcen, P. O. Box 119, 13000 Tlemcen, Algeria*
[c]*Department of Chemistry, Faculty of Science, Ain Shams University, Cairo 11566, Egypt*

Severe exposure can lead to collapse or even fatal outcomes. These compounds are highly soluble and persist at high concentrations in industrial wastewater, posing significant environmental challenges. As a result, the removal of nitrophenols from wastewater is essential.

To overcome these limitations, magnetic ferrite-based nanomaterials, particularly nickel ferrite ($NiFe_2O_4$), have emerged as promising alternatives. Ferrites exhibit superior redox properties, high surface area, low band gap energy, and excellent magnetic separability, which significantly enhance their catalytic performance while enabling easy post-treatment recovery using an external magnetic field.[5–7] Ferrites have also shown potential in applications such as dye degradation, sensing, drug delivery, and water splitting, demonstrating their multifunctionality and stability.[8,9]

Several remediation methods, including, catalytic reduction,[10] adsorption,[11] photodegradation,[12] and membrane filtration,[13] have been employed. However, these approaches often suffer from high costs and limited removal efficiency.

In catalytic decomposition, traditional catalysts like, carbon nanotubes,[14] activated carbon,[15] oxides,[16] and microporous polymers[17] have been widely utilized. However, these materials present a significant limitation in practical applications due to challenges in separating them from the treated water. This issue becomes particularly problematic in large-scale systems. The incomplete removal of these conventional catalysts from the processed solution can result in their buildup in the environment, potentially causing secondary pollution and introducing new environmental contaminants. The issue has been effectively addressed with the development of magnetic nanocatalysts, which have garnered significant research attention for reducing organic contaminants from wastewater. These materials offer unique advantages, such as a low band gap energy, high reduction capacity, and effortless separation using an external magnetic field. This minimizes the risk of secondary pollution, overcoming the limitations of traditional catalysts that are difficult to separate from contaminated solutions. Recent research has demonstrated that $NiFe_2O_4$ nanostructures can effectively catalyze the reduction of nitroaromatic compounds such as 4-NP under visible light or mild reaction conditions.[18,19] However, bare ferrite nanoparticles often suffer from agglomeration, poor dispersibility in aqueous systems, and reduced active site accessibility, which limit their catalytic efficiency.[20] To address this, researchers have begun incorporating conductive polymers—such as polyaniline (PANI), polypyrrole (PPy), and their derivatives—onto ferrite surfaces to form hybrid nanocomposites with enhanced performance.[7,20] They have been utilized in diverse applications, including dye degradation, electrochemical sensors, cancer treatment, drug delivery, gas sensing, and water splitting, owing to their high surface area and stability. Jiang *et al.* (2025) demonstrated high catalytic performance using core–shell magnetic heterojunctions for 4-NP reduction under visible light.[21] Similarly, Chen *et al.* (2025) reported a bifunctional $NiFe_2O_4$@graphene nanocomposite with enhanced stability and reusability.[22] Their potential for nitro compound removal in wastewater treatment makes them an attractive choice.

Moreover, there is growing interest in enhancing the performance of these magnetic nano-catalyst by incorporating conductive polymers like polyaniline (PANI)[23] and polypyrrole (PPy).[24] These polymers contribute additional benefits, including a low gap energy, flexibility, robust mechanical strength, and distinctive electrical properties, along with functional groups such as –NH. Several studies have highlighted that conductive polymer coatings not only reduce particle agglomeration but also improve charge carrier separation and redox kinetics, especially in ferrite-based nanocomposites.[25,26] These ferrite–polymer nanocomposites benefit from improved electrical conductivity, enhanced charge separation, redox tunability, and better stability in aqueous environments. In particular, polymers like poly(aniline-*co*-*o*-toluidine) (PAOT) possess –NH and $-CH_3$ functional groups that enhance electron delocalization and create strong interfacial interactions with ferrite nanoparticles. Such synergy facilitates electron transfer processes crucial to catalytic reduction reactions.[19,20]

Magnetic ferrite-based systems such as $NiFe_2O_4$ have been extensively utilized in various domains including dye degradation,[27] electrochemical sensors,[28] cancers treatment,[29] drug delivery,[30] gas sensing[31] and water splitting,[32] owing to their stability, high surface area, and electron transfer capabilities.

Despite their potential, $NiFe_2O_4$-based polymer nanocomposites remain underexplored for catalytic detoxification of 4-NP. Previous studies have largely focused on either bare ferrites or composites with conventional polymers. Furthermore, detailed mechanistic studies on the role of polymer-ferrite interfacial bonding, surface charge modulation, and catalyst recyclability in enhancing 4-NP reduction remain scarce. While magnetic $NiFe_2O_4$ nanoparticles have shown promise in pollutant degradation, there remains a significant gap in understanding how copolymer-functionalization, particularly with PAOT, can be leveraged to maximize their performance in wastewater treatment applications. No comprehensive studies have yet reported the synthesis, stability, and catalytic behavior of $NiFe_2O_4$/PAOT nanocomposites toward 4-NP reduction under mild conditions.

In this study, a $NiFe_2O_4$/PAOT nanocomposite was developed by first synthesizing $NiFe_2O_4$ nanoparticles and subsequently modifying them with poly(aniline-*co*-*o*-toluidine) (PAOT). The $-CH_3$ group in the *o*-toluidine aromatic ring enhances electron density, facilitating strong interactions between nickel ferrite molecules and the polymer.[33,34] These non-covalent interactions, particularly between the hydrogen of the metal complex and the electron-rich *o*-toluidine ring, contribute to the nanocomposite's enhanced stability. The use of magnetic metal ferrites, particularly nickel ferrite combined with poly(aniline-*co*-*o*-toluidine), offers notable advantages such as cost-effectiveness, high reduction efficiency, and straightforward preparation, making them highly suitable catalysts for the reduction of 4-nitrophenol. These catalysts have demonstrated significant effectiveness in addressing the challenges associated with 4-nitrophenol reduction. Furthermore, this approach highlights the potential of ferrite-poly(aniline-*co*-*o*-toluidine) composites synthesized through chemical polymerization,

which, to the best of our knowledge, remain relatively underutilized for this application.

Experimental

Chemicals and apparatus

All chemicals were utilized as received without additional purification. Ferric chloride hexahydrate ($FeCl_3 \cdot 6H_2O$, 97%) and nickel chloride hexahydrate ($NiCl_2 \cdot 6H_2O$) were sourced from Sigma-Aldrich, USA. Ammonium persulfate ($(NH_4)_2S_2O_8$), aniline ($C_6H_5NH_2$), and *o*-toluidine (C_7H_9N) were also obtained from the same supplier. Sodium hydroxide (NaOH) and hydrochloric acid (HCl) were procured from Merck, Germany. 4-Nitrophenol ($C_6H_5NO_3$) was acquired from, FLUKA Chemika, Switzerland. All reagents were of analytical grade. Ultrapure water was used for all solution preparations. Both stock and diluted, 4-NP solutions were stored in dark, airtight containers to avoid degradation.

For the instruments, FTIR spectrometer (Sp-3-300, Pye-Unicam, UK) was recorded between wave numbers of 200 and 4000 cm^{-1}. XRD analysis (ULTIMA IV, Rigaku, JAPAN), SEM analysis (JSM-IT800, JEOL Ltd, JAPAN) to examine the surface texture and porosity development, EDX analysis (JSM-IT800, JEOL Ltd, JAPAN), UV-Vis-NIR spectrophotometer (UV-3600, SHIMASZU, JAPAN), UV-visible spectrophotometer (GENESYS 10S, USA).

Synthesis of nano-sized nickel ferrite ($NiFe_2O_4$)

At room temperature (22 ± 2 °C), a solution was prepared using ferric and nickel chloride in a 2 : 1 molar ratio and stirred continuously for 30 min. A 2.0 M sodium hydroxide (NaOH) solution was then gradually introduced at a controlled rate of 1.0 mL min^{-1} until the pH of the mixture reached.[35] The reaction led to the formation of a brown precipitate (Scheme 1), which was subsequently heated to 100 °C while being stirred for one hour. The mixture was then left to mature overnight. The precipitate was thoroughly washed with distilled water until the filtrate reached a neutral pH of 7. The obtained residue was dried at 110 °C for six hours, transforming into a deep dark powder, which was then subjected to calcination at 600 °C for five hours. The final product was ground and stored in a desiccator for further use.

Synthesis of $NiFe_2O_4$/PAOT nanocomposite

Nickel ferrite-based polymer nanocomposites were synthesized through a chemical polymerization process (Scheme 2). Initially, 4.5 g of $NiFe_2O_4$ nanoparticles were dispersed in a solvent mixture containing 20 mL of chloroform and 30 mL of double-distilled water. This dispersion was subjected to ultrasonic treatment for 1 hour at room temperature (22 ± 2 °C). Concurrently, 0.05 moles of both aniline and *o*-toluidine monomers were dissolved in 200 mL of 1.0 M hydrochloric acid and stirred continuously for 30 min. The nanoparticle dispersion was then combined with the monomer solution and further sonicated for 30 minutes. Polymerization was initiated by the dropwise addition of 20 mL of a 0.1 M aqueous ammonium persulfate (APS) solution at a controlled rate of 0.5 mL min^{-1} using a peristaltic pump, while sonication continued for an additional hour. A gradual change to a black coloration was observed during the process.[36] The reaction mixture was left undisturbed overnight. The resulting nickel ferrite-poly(aniline-*co*-*o*-toluidine) composite was separated by vacuum filtration, thoroughly washed with double-distilled water and methanol, and subsequently dried at 60 °C. The final dried product was finely ground into powder for further use.

Catalytic reduction of nitrophenol

The reduction efficiency of the synthesized nanocomposites was evaluated using the batch equilibrium method. A series of 4-

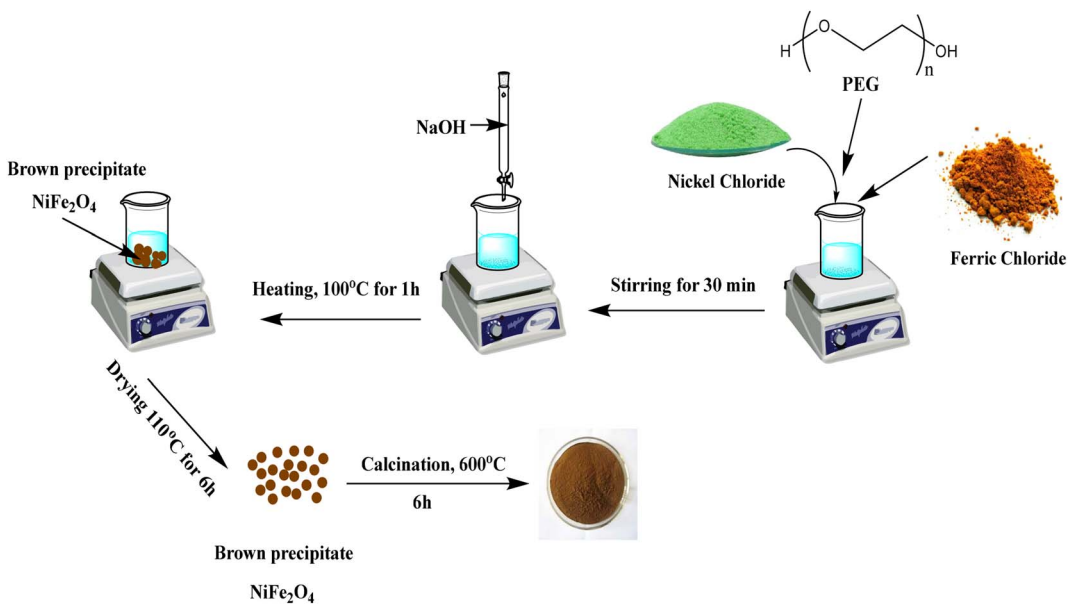

Scheme 1 Schematic representation the preparation of $NiFe_2O_4$ nanoparticles.

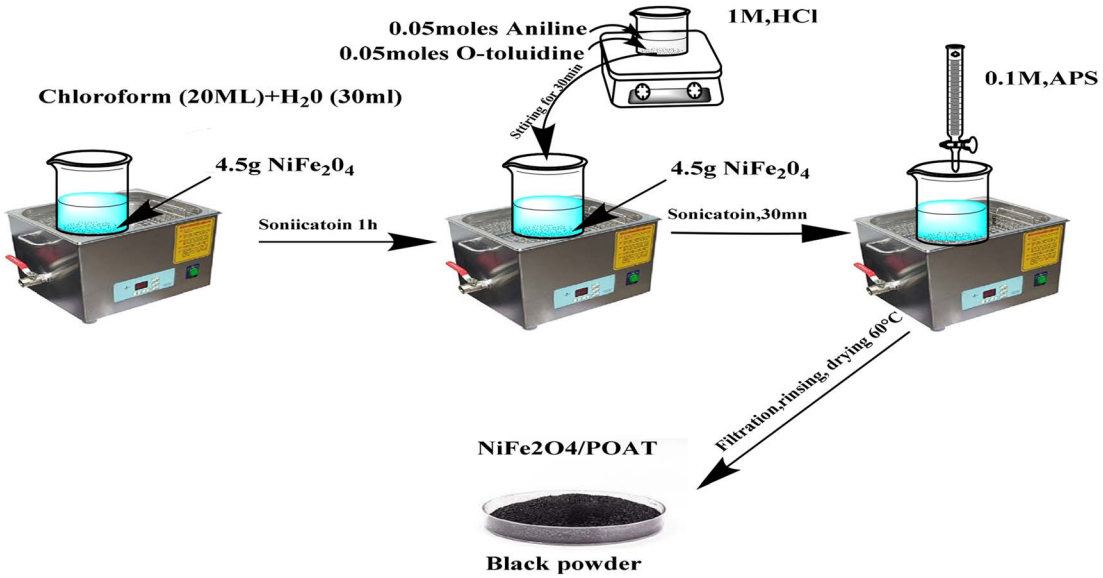

Scheme 2 Schematic representation the preparation of $NiFe_2O_4$/PAOT nanocomposite.

nitrophenol (4-NP) solutions with concentrations of 2, 10, and 15 ppm were prepared. Varying amounts (5, 10, and 20 mg) of the $NiFe_2O_4$/PAOT nanocomposite were dispersed in 10 mL of the prepared 4-NP aqueous solution, maintaining a pH of 7.43. The reaction mixtures were allowed to interact for durations ranging from 2 to 60 minutes at a constant temperature of 25 °C. After the reaction, the $NiFe_2O_4$/PAOT catalyst was separated by centrifugation, with additional recovery facilitated using a magnetic bar. The conversion of 4-nitrophenol (4-NP) to 4-aminophenol (4-AP) was quantitatively analyzed using spectrophotometry. The maximum absorption wavelength (λ_{max}) was recorded at 400 nm for 4-NP and 318 nm for 4-AP.

Results and discussion

Characterization of the nanomaterial composite

Fourier transform infra-red (FT-IR) spectroscopy. Fig. 1 presents the FTIR spectra of $NiFe_2O_4$ nanoparticles post-calcination and the $NiFe_2O_4$/PAOT nanocomposite after copolymerisation. The IR spectrum of calcined $NiFe_2O_4$ (ref. 37) nanoparticles shows a thin, broad band at about 3440 cm^{-3}. This band shows the O–H stretching and vibrational modes of the water that is adsorbed in the KBr pellet manufacturing process. The asymmetric stretching vibrations of the adsorbed carbonate groups account for two additional bands located between 1632 and 1382 cm^{-1}. The characteristic bands seen at 585–453 cm^{-3} are caused by the intrinsic stretching vibrations of the Fe–O and Ni–O bonds in the spinel structure. The spectra of calcinated $NiFe_2O_4$ nanoparticles exhibit no additional peaks.[38] On the other hand, the infrared spectrum of the $NiFe_2O_4$/poly(aniline-*co*-*o*-toluidine) composite shows a broad band in the 3384–3230 cm^{-3} range. This band is due to N–H stretching, which is made wider by hydrogen bonding. A band seen between 2920 and 2852 cm^{-3} shows the stretching vibrations of the $-CH_3$ group in the toluidine moiety. The bands observed in the 1587–1485 cm^{-1} region are attributed to the stretching vibrations of N–H and C=N. Bands present in the 1149–1006 cm^{-1} range are linked to the bending of the C–H plane. Finally, the metal–oxygen vibrations in the spinel crystal lattice are linked to two separate bands that span from 572 to 415 cm^{-3}.

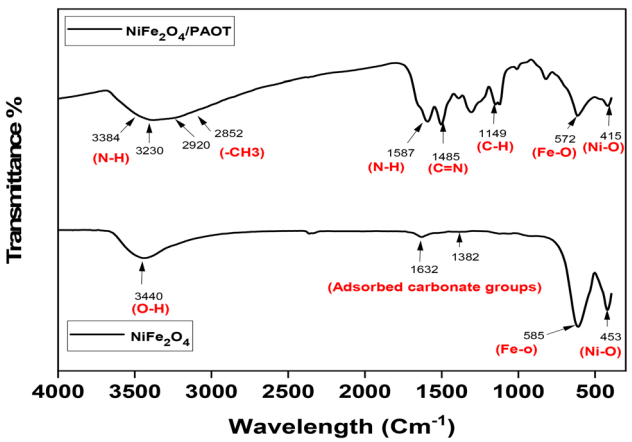

Fig. 1 FTIR spectra of $NiFe_2O_4$ nanoparticles and $NiFe_2O_4$/PAOT nanocomposite.

SEM microscopic analysis. The unique morphological features of $NiFeO_4$ are revealed by the SEM image Fig. 2(a), which emphasises homogeneous particle distribution and nanoscale structure. The distribution of the particle sizes is rather uniform and homogeneous, ranging from roughly 45 nm to 56 nm. This nanoscale size can increase the material's surface area, which is essential to its catalytic and magnetic capabilities. High-quality $NiFeO_4$ synthesis is demonstrated by the tightly packed particle arrangement with little agglomeration. Applications like adsorption, catalytic reduction, and other environmental cleanup procedures benefit from this morphology.[39]

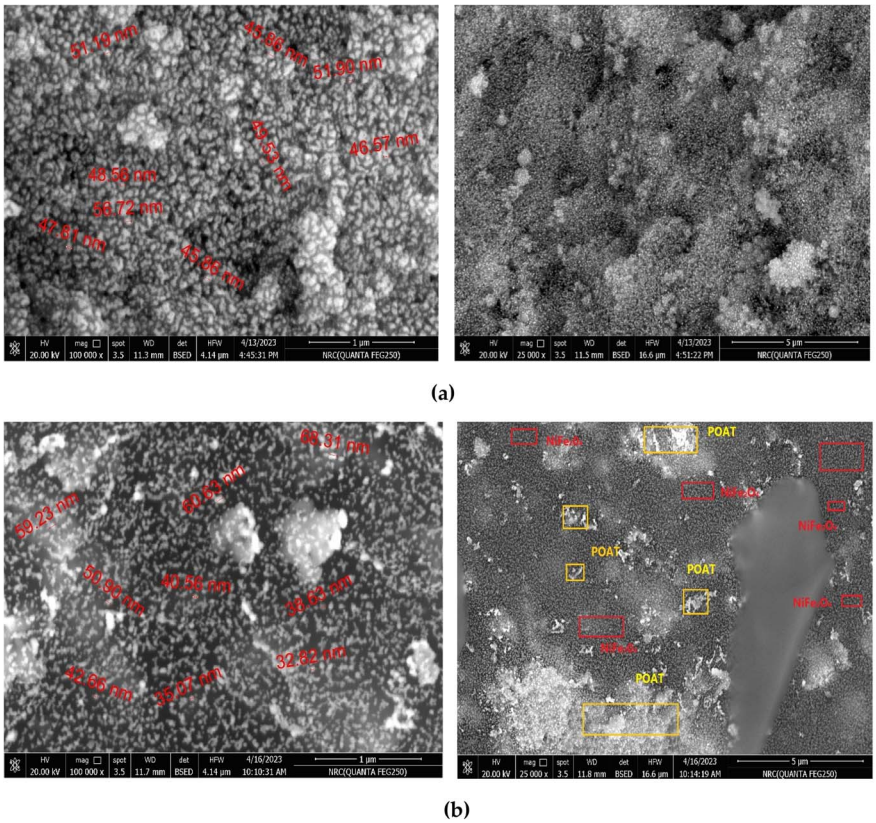

Fig. 2 SEM images of (a) $NiFe_2O_4$, and (b) $NiFe_2O_4$ coated with poly[*co*-*o*-toluidine + aniline].

The SEM image in Fig. 2(b), recorded at a scale of 1 μm, shows the structural and morphological changes in $NiFe_2O_4$ coated with poly(*o*-toluidine-*co*-aniline), resulting from the presence of the polymer.[40] The histograms in Fig. 3 shows the particle sizes vary from about 32 nm to 68 nm, suggesting that the polymer coating causes variations in the distribution. The polymer produces a smoother and more cohesive surface morphology, and the image shows a rather uniform dispersion of particles. The polymer's presence is probably what improves material stability and decreases particle aggregation. While preserving the fundamental nanoscale characteristics of $NiFeO_4$, this coating adds novel surface characteristics that are beneficial for catalytic and environmental applications.

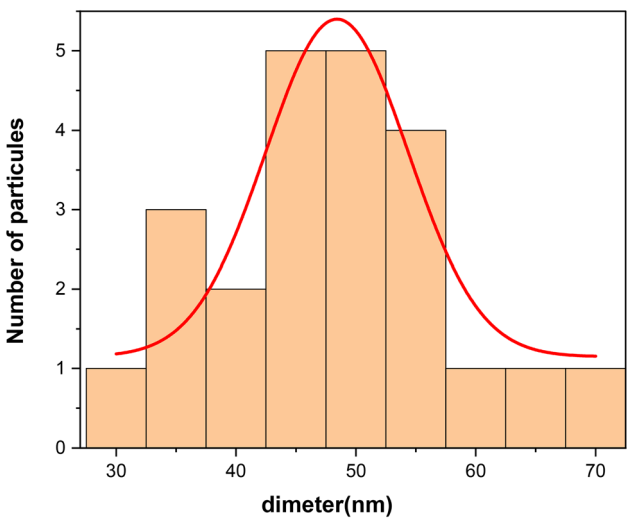

Fig. 3 Particle size distribution histogram of $NiFe_2O_4$ and $NiFe_2O_4$ coated with poly(aniline-*co*-*o*-toluidine) based on SEM analysis.

EDX spectrum. The EDX analysis in Fig. 4 showed that the synthesis and surface modification went well by confirming the elemental makeup of $NiFe_2O_4$ and its polymer-coated form. Following the expected spinel structure, the analysis found that $NiFe_2O_4$ is mostly made up of oxygen, iron, and nickel. Iron had the highest weight percentage (62.71%), indicating its dominant presence in the structure, but oxygen had the lowest weight percentage (26.15%) due to its lower atomic mass. The expected stoichiometric ratio was met by the smaller amounts of nickel (11.13% by weight). Iron and oxygen have modest error margins, indicating accurate measurements. Because lighter elements like carbon and nitrogen were incorporated from the polymer layer, the atomic percentages of metal elements in the polymer-coated $NiFe_2O_4$ sample fell. Furthermore, trace levels of chlorine were found, indicating the presence of small amounts of residual contaminants. The results showed that the polymer coating changed the surface by adding lighter parts while keeping the spinel structure of the core material.

Powder X-ray diffraction (XRD) analysis. The synthesized materials were subjected to analysis of their structural

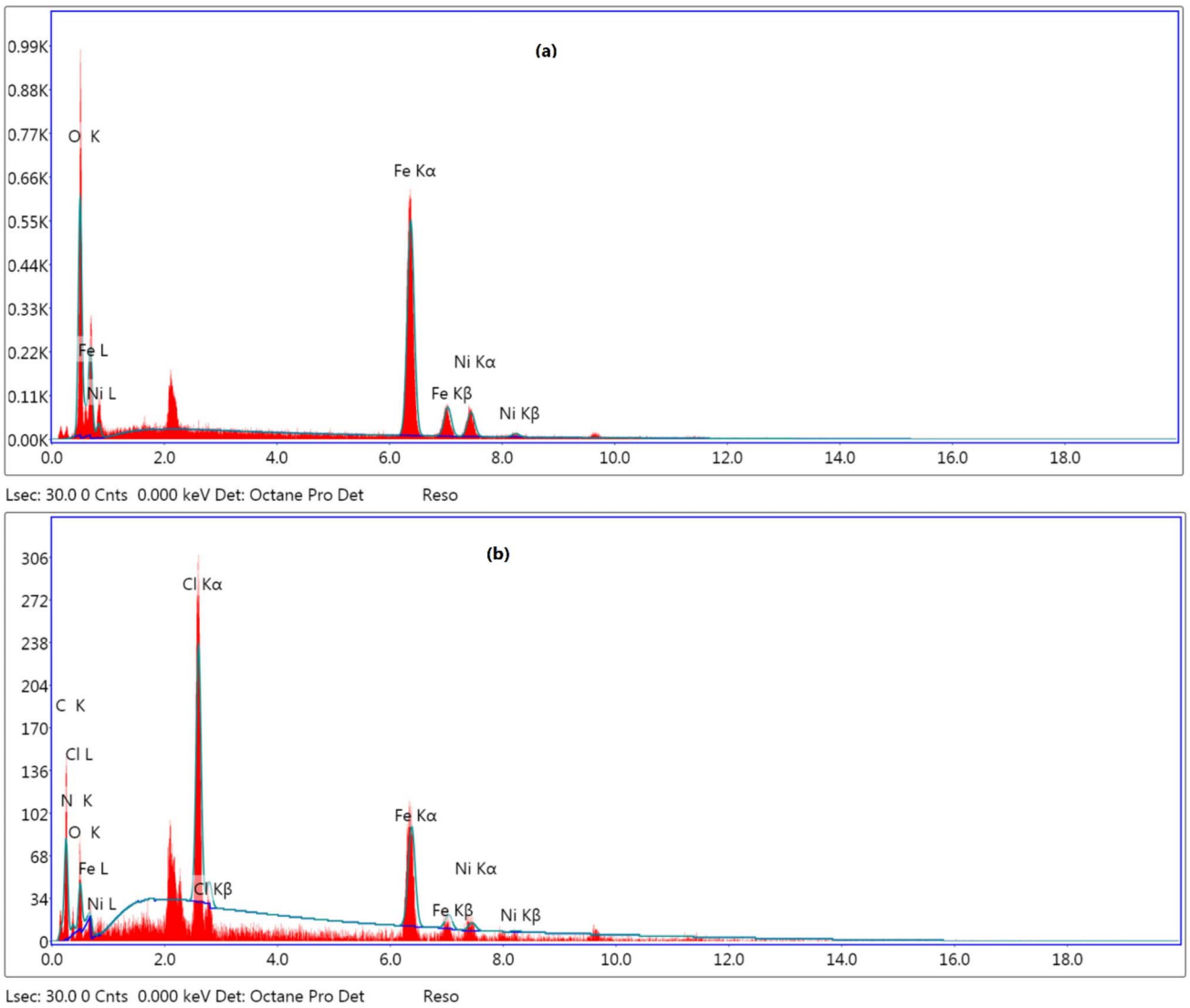

Fig. 4 (a) EDX of $NiFe_2O_4$ (a), (b) EDX spectrum of $NiFe_2O_4$ coated with poly(aniline-*co*-*o*-toluidine).

properties through X-ray diffraction (XRD). XRD patterns for $NiFe_2O_4$ nanoparticles[37] and $NiFe_2O_4$/PAOT nanocomposites were acquired using a powder X-ray diffractometer (PANalytical, Almelo, Netherlands) with CuKα radiation ($\lambda = 0.154$ nm) across a scanning range of 10° to 70°. The diffraction patterns, in accordance with the JCPDS standard (card no. 10-0325), confirmed the formation of a cubic spinel crystal structure, as depicted in Fig. 5.[36,37] No further peaks suggesting the presence of impurities like NiO or FeO_3 were detected. Polymer-enhanced nickel ferrite catalysts for the efficient reduction of 4-nitrophenol pollutants. Seven important diffraction peaks were found at 2, values of 30.24°, 35.48°, 36.94°, 43.06°, 53.80°, 57.20°, and 62.88°, corresponding to the crystal planes (311), (220), (222), (422), (511), (400), and (440). The XRD pattern of $NiFe_2O_4$/PAOT nanocomposites was mostly the same as that of pure $NiFe_2O_4$ nanoparticles, with the addition of a broad diffraction band seen between $2\theta = 15°$ and 25.[36] This was because the PAOT copolymer matrix is amorphous in Fig. 5.[36] The observed decrease in diffraction peak intensities in the nanocomposite relative to the pure $NiFe_2O_4$ nanoparticles suggests that PAOT was successfully integrated onto the $NiFe_2O_4$ surface while maintaining its crystalline structure. The average particle sizes of $NiFe_2O_4$ and $NiFe_2O_4$/PAOT were estimated using Scherrer's equation.

$$D = (K\lambda)/(\beta\cos\theta) \quad (1)$$

The Scherrer equation defines D as the crystallite size, λ as the wavelength of the X-ray radiation (CuKα, 0.154 nm), θ as the Bragg diffraction angle (in radians), and β as the full width at half maximum (FWHM) of the most intense XRD peak, particularly for the (311) plane. The value of the Scherrer constant (k) was set at 0.9. The calculation method yielded estimated average crystallite sizes of 12.3 nm for $NiFe_2O_4$ nanoparticles and 16.7 nm for $NiFe_2O_4$/PAOT nanocomposites.[36]

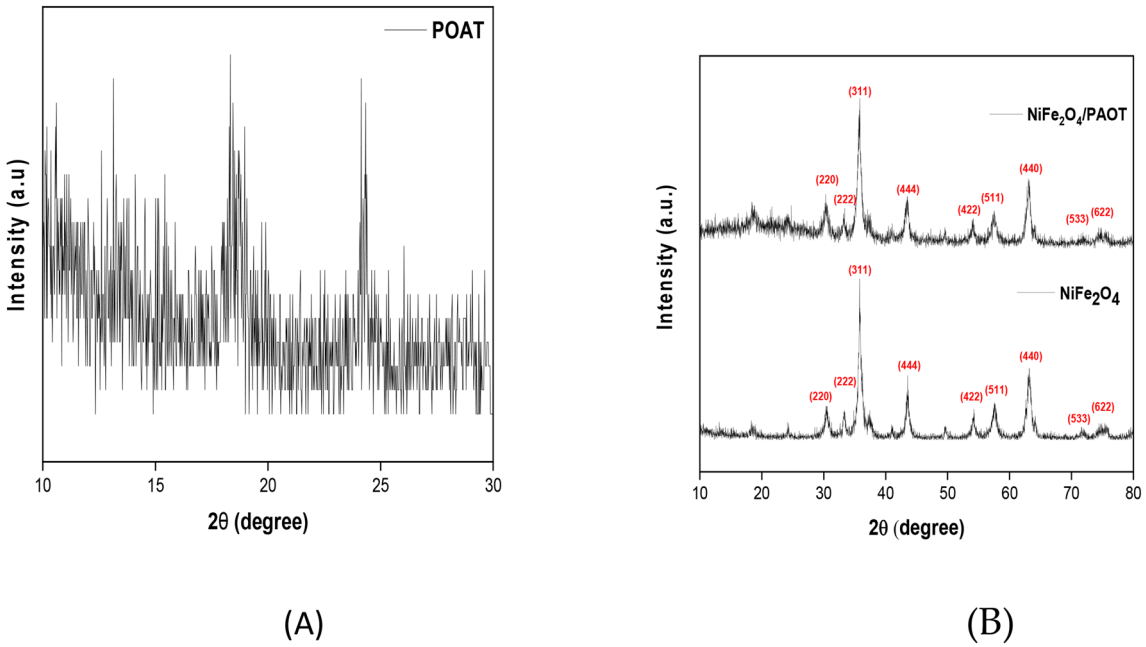

Fig. 5 XRD patterns of (A) PAOT, and (B) $NiFe_2O_4$ nanoparticles and $NiFe_2O_4$/PAOT nanocomposite.

In both the bare $NiFe_2O_4$ and the $NiFe_2O_4$/PAOT nanocomposite, additional diffraction peaks are observed in the high-angle region between 70° and 80° (2θ). These peaks correspond to the (533) and (622) crystallographic planes of the spinel $NiFe_2O_4$ phase, in agreement with the standard JCPDS card no. 10-0325. The presence of these reflections in both samples confirms that the crystalline spinel structure of $NiFe_2O_4$ is retained after polymer coating. The PAOT modification does not introduce new crystalline peaks in this range, indicating that the polymer layer is amorphous in nature and does not alter the fundamental crystal lattice of the ferrite core.

Catalytic degradatoin of 4-nitrophenol (NP). The process of catalytic reduction stands as the most effective method for converting hazardous nitrophenols, exemplified by 4-nitrophenol (4-NP), into benign aminophenols. Solutions that incorporate 4-NP display an absorbance peak within the range of 300 to 400 nm, with distinct absorption maxima identified at 400 nm for 4-NP and at 318 nm for 4-aminophenol (4-AP), as illustrated in Fig. 6. Upon the introduction of $NiFe_2O_4$ coated with poly[*o*-toluidine + aniline], the solution exhibited a discernible colour transition from dark yellow to light yellow within a span of 60 min.

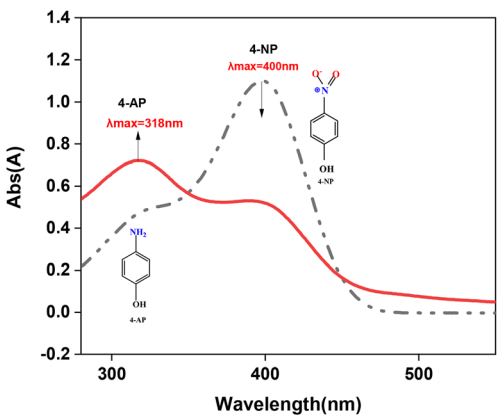

Fig. 6 Absorption peaks of 4-nitrophenol and 4-aminophenol in UV-Vis spectrum.

Solutions with concentrations of 2, 10, and 15 ppm were employed to investigate the catalytic reduction of 4-NP in 10 mL. Due to the magnetic properties of the materials, we implemented a glass stirrer to ensure homogenous suspension agitation. 10 mg of the catalyst was introduced after five minutes of continuous agitation, and the mixture was stirred for an additional 60 min at room temperature thereafter. The darker yellow colouration progressively dissipated during this period. Molecular absorption spectroscopy was employed to monitor the absorbance at 400 nm in order to ascertain the conversion of 4-NP to 4-AP. The relative concentration of 4-NP was then calculated using the following formula:[41]

$$C_t/C_0 = I_t/I_0 \quad (2)$$

The C_0 (mg L^{-1}) value shows how much 4-NP was in the solution before the catalyst was added. The C_t (mg L^{-1}) value shows how much 4-NP was still in the solution at a certain time after the catalyst was added. I_0 and I_t represent the absorbance intensities of 4-NP measured at 400 nm at $t = 0$ (prior to the addition of the catalyst) and at any later reaction time, respectively. The intensities were presumed to have a direct correlation with the concentration of 4-NP in the reaction system.

Effect of 4-NP concentration. The catalytic reduction of 4-nitrophenol (4-NP) to 4-aminophenol (4-AP) was examined using $NiFe_2O_4$ coated with poly[*o*-toluidine + aniline]. The study was conducted at initial concentrations of 2 ppm, 10 ppm, and

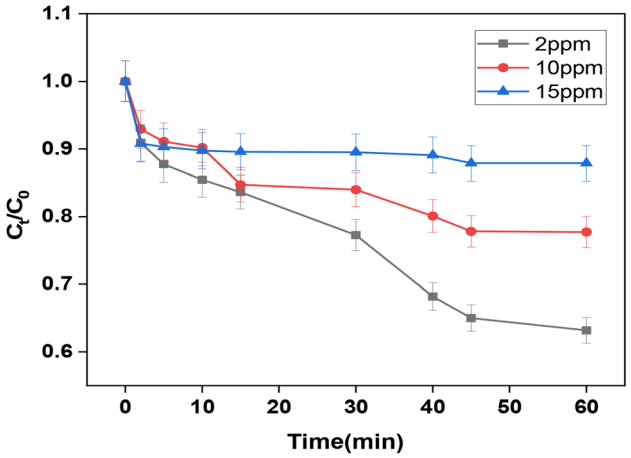

Fig. 7 Effect of $C_{NiFe_2O_4/PAOT}$ on the reduction of (4-NP) [$V_{solution}$ = 10 mL, T = 25 °C, pH = 7.43, [4-NP] = 2, 10, 15 ppm; m = 10 mg].

15 ppm over a reaction period of 60 min using a catalyst dosage of 10 mg, as shown in Fig. 7. At a starting concentration of 2 ppm, the reduction happened faster, as shown by a steeper drop in the C_t/C_0 ratio to 0.631. This means that the catalyst was more effective at lower substrate concentrations. At 10 ppm, the reaction rate exhibited a moderate level, with a more gradual decline in C_t/C_0 relative to 2 ppm, reaching a value of 0.77, indicating a reduction in catalytic activity with increasing concentration. At a concentration of 15 ppm, the reaction progressed most slowly and exhibited the lowest reduction efficiency at equilibrium. After 60 min, the C_t/C_0 ratio was 0.878. Since the catalyst dose was only 10 mg, higher concentrations of 4-NP may stop the reaction. This is probably because the active site is full or there are problems with mass transfer.

The $NiFe_2O_4$/POAT catalyst's conduction band acts as an electron source, allowing interactions between active electrons (e^-) and 4-NP. These interactions help reduce the $-NO_2$ group to $-NH_2$ by moving electrons and protons around. $NiFe_2O_4$/POAT has a low energy band gap, which makes it easier for 4-NP to turn into 4-AP. This is done by efficiently moving electrons between the catalyst and the pollutant, which speeds up the reaction. The polymer layer enhances electron mobility between the catalyst and 4-NP, thereby increasing its catalytic activity. However, this enhancement decreases when the system is saturated or overloaded, resulting in a decline in catalytic efficiency.[42]

Fig. 7 illustrates the spectral evolution of the 4-NP reduction reaction. At 0 minutes, the absorbance peak at 400 nm reaches its maximum, signifying the initial concentration of 4-NP. During the reaction, the peak at 400 nm diminishes progressively, whereas the peak at 318 nm rises, indicating the transformation of 4-NP to 4-AP. At 2 ppm, the absorbance curve drops more quickly at 400 nm than at 10 ppm and 15 ppm. This means that the reaction happens faster at lower concentrations. The observed trends indicate that $NiFe_2O_4$/POAT shows superior catalytic performance at lower concentrations, as diminished competition for active sites enhances electron transfer and reaction advancement.

Fig. 8 illustrates the time-dependent UV-visible spectral changes during the catalytic reduction of 4-nitrophenol (4-NP) to 4-aminophenol (4-AP) using $NiFe_2O_4$/PAOT nanocomposites at initial concentrations of (a) 2 ppm, (b) 10 ppm, and (c) 15 ppm. At the start of the reaction (t = 0 min), a strong absorbance peak is observed at 400 nm in all spectra, corresponding to the 4-nitrophenolate ion. As the reaction proceeds, the intensity of this peak gradually decreases, indicating the progressive consumption of 4-NP. Simultaneously, a new peak appears around 318 nm, which corresponds to the formation of 4-aminophenol (4-AP), the final reduction product. The rate of peak reduction is more rapid at lower concentrations (2 ppm), suggesting enhanced catalytic activity due to reduced competition for active sites. At higher concentrations (10 and 15 ppm), the peak reduction is slower, indicating a concentration-dependent reaction rate. The spectral shift and disappearance of the 400 nm peak, accompanied by the emergence of the 318 nm band, provide clear evidence for the successful transformation of 4-NP into 4-AP, demonstrating the efficiency of $NiFe_2O_4$/PAOT as a visible-light-responsive catalyst under ambient conditions.

Kinetics of the reduction process of nitrophenol. The reduction rate of nitrophenol can be analyzed using a pseudo-first-order kinetic model, as described in prior studies.[43] For the 4-nitrophenol (4-NP) reduction process, the ratio of the concentration of 4-NP at any time t (C_t) to its initial concentration at t = 0 (C_0) is equivalent to the ratio of the corresponding absorbance values A_t/A_0 measured at a wavelength of 400 nm. Based on this relationship, the kinetic equation governing the reduction process can be expressed bu eqn (3):[44]

$$-\ln(C_t/C_0) = -\ln(A_t/A_0) = K_{app}t \quad (3)$$

The apparent rate constant (K_{app}) can be calculated from the slope of the linear graph of $\ln(C_t/C_0)$ *versus* reaction time. Fig. 9 demonstrates a linear relationship between $\ln(A_t/A_0)$ and time, confirming that the reduction of 4-NP using $NiFe_2O_4$/POAT followed pseudo-first-order kinetics. Furthermore, the catalytic reduction of 2-NP with $NiFe_2O_4$/POAT was also examined. Fig. 9 illustrates that the linear trend of $\ln(A_t/A_0)$ against time also suggests that the reduction of 2-NP adhered to pseudo-first-order kinetics. The apparent rate constants (K_{app}) are calculated based on the slopes of the corresponding lines. At 2 ppm ($K_{app} = 1.16 \times 10^{-2}$ min^{-1}, $R^2 = 0.98$), 10 ppm ($K_{app} = 3.5 \times 10^{-3}$ min^{-1}, $R^2 = 0.96$), 15 ppm ($K_{app} = 5.44 \times 10^{-4}$ min^{-1}, $R^2 = 0.94$) dependency on concentration: the reduction rate exhibits significant variation as initial concentrations increase. This change could be caused by differences in how easy it is to get to active sites on the catalyst or by changes in how the 4-NP molecules interact with the surface of the catalyst.

Effect of the catalyst dose. Fig. 10 shows how the amount of $NiFe_2O_4$/PAOT catalyst affects the breakdown of 4-nitrophenol (4-NP). This evaluation was conducted at various initial concentrations (2 ppm, 10 ppm, and 15 ppm) with catalyst amounts of 5 mg, 10 mg, and 20 mg. An increase in catalyst mass led to a decrease in the C_t/C_0 ratio (where C_t denotes the remaining 4-NP concentration and C_0 is the initial

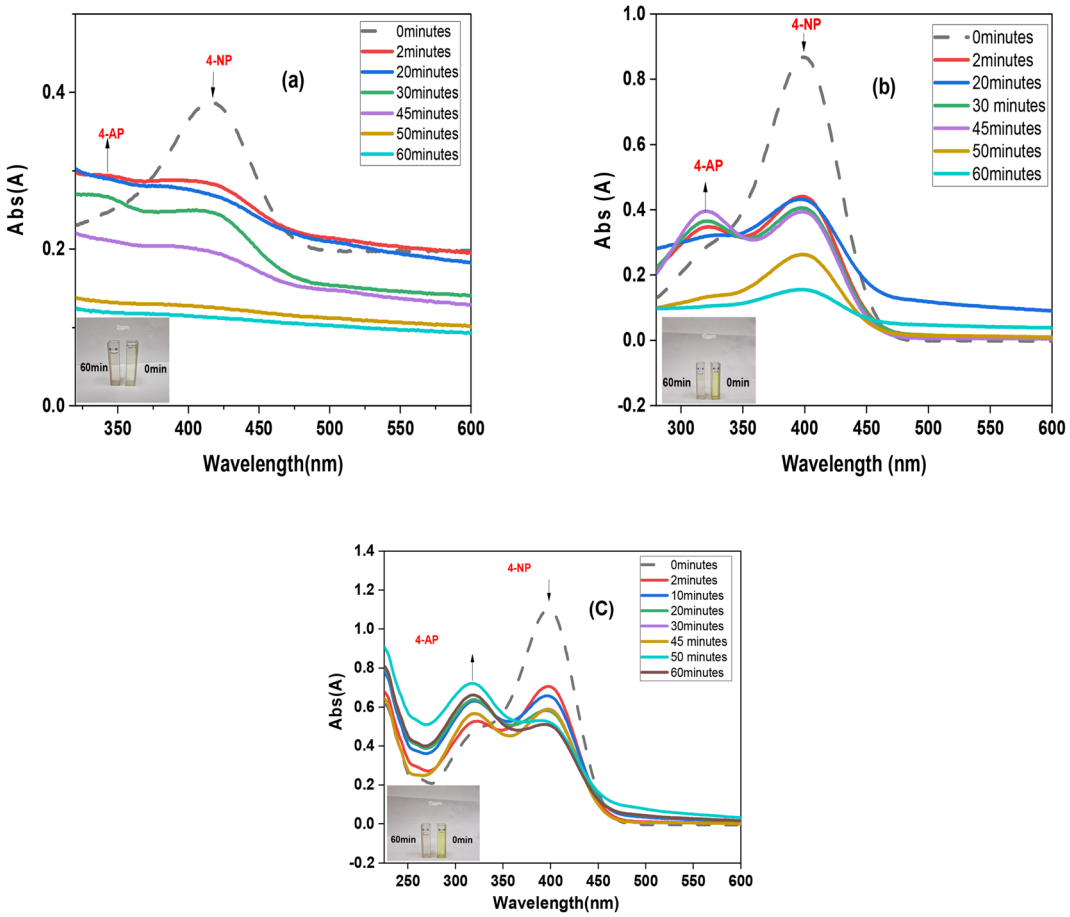

Fig. 8 UV-visible spectra of the reduction reaction of 4-NP to 4-AP at (a) 2 ppm, (b) 10 ppm, and (c) 15 ppm.

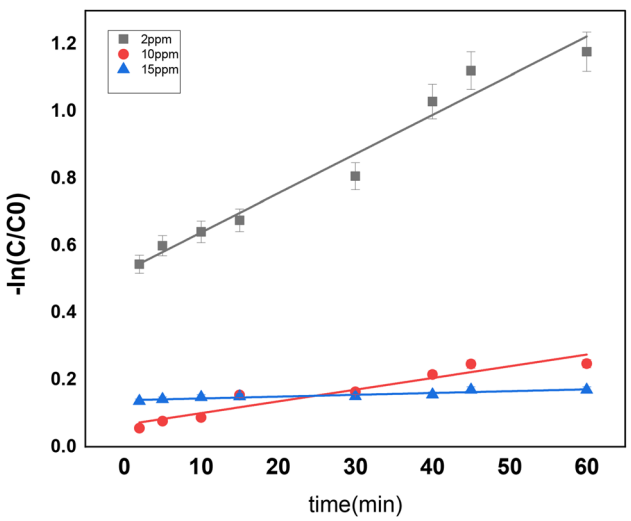

Fig. 9 Rate of reduction of 4-nitrophenol at different concentrations using 10 mg of $NiFe_2O_4$/POAT.

concentration), suggesting enhanced reduction efficiency. The 2 ppm solution exhibited the most notable reduction, with the C_t/C_0 ratio dropping to 0.545 at 20 mg of catalyst, indicating a highly effective degradation process. A comparable trend was noted for the 10 ppm and 15 ppm solutions, with the C_t/C_0 ratio reducing to 0.59 and 0.78, respectively, at 20 mg of catalyst. Nonetheless, the degree of reduction appeared to diminish at elevated concentrations, indicating that a larger catalyst dosage is necessary for efficient reduction as pollutant levels rise. The findings highlight that increasing the catalyst dose improves

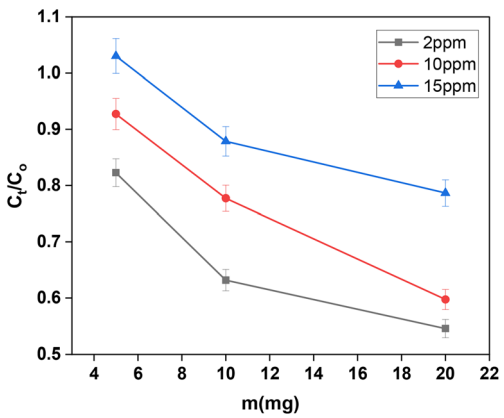

Fig. 10 Effect of dose ($NiFe_2O_4$/PAOT) on the reduction of (4-NP): $V_{solution} = 10$ mL, $T = 25$ °C, pH = 7.43, [4-NP] = 2, 10, 15 ppm, $m = (5, 10, 20)$ mg.

reduction efficiency, with a more pronounced effect observed at lower pollutant concentrations. At higher concentrations, the efficiency gain diminishes, highlighting the importance of optimizing catalyst dosage based on pollutant levels for maximum effectiveness.[45]

Temperature effect. The reduction efficiency of 4-nitrophenol (4-NP) was assessed at two temperatures, 37 °C and 50 °C, employing $NiFe_2O_4$/POAT as a catalyst, as illustrated in Fig. 11. The findings demonstrate that temperature significantly influences the reduction process. At 37 °C, the reduction efficiency is comparatively lower, with 2 ppm reaching a maximum efficiency of over 64%. In contrast, higher concentrations of 10 ppm and 15 ppm yield efficiencies of 38% and 37%, respectively. At 50 °C, the efficiency reduction markedly enhances, achieving 64% for 2 ppm, 63% for 10 ppm, and 61% for 15 ppm, indicating a more effective catalytic process. Elevated temperatures augment the kinetic energy of reactant molecules, facilitating their interaction with the active electrons of $NiFe_2O_4$/POAT. Moreover, increased temperatures may enhance the electron transfer process from 4-NP to 4-AP, which is a vital component of the reduction mechanism. The findings indicate that the reduction of 4-NP is influenced by temperature, with elevated temperatures enhancing catalytic performance. The results suggest that 50 °C may be an optimal temperature for maximizing reduction efficiency under the specified reaction conditions.[46,47]

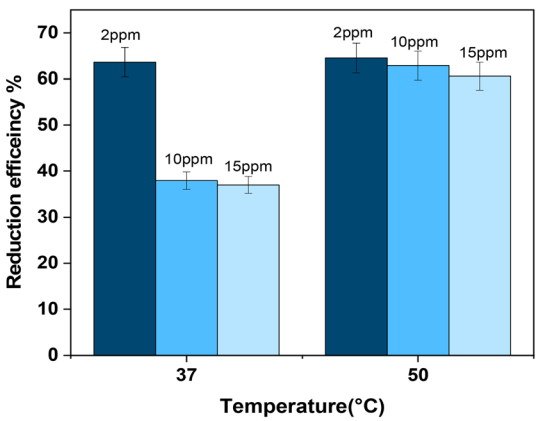

Fig. 11 Effect of temperature on the reduction of 4-NP [$V_{solution}$ = 10 mL, T = (37, 50) °C, pH = 7.43, [4-NP] = 2, 10, 15 ppm].

Catalyst optimization. The UV-visible absorption spectra illustrate the catalytic reduction of 4-NP to 4-AP under optimal conditions, utilising 20 mg of $NiFe_2O_4$/POAT as a catalyst at 50 °C, as shown in Fig. 12. The research was carried out using various initial concentrations of 4-NP (2 ppm, 10 ppm, and 15 ppm) and documented at two time points: t = 0 min and t = 60 min. At the initiation of the reaction (t = 0 min), all samples exhibited a pronounced absorption peak at 400 nm, indicative of the nitrophenolate ion, which represents the characteristic form of 4-NP under alkaline conditions. The absorbance intensity exhibited an increase corresponding to higher concentrations of 4-NP, with the maximum observed for the 15 ppm solution. Following a 60 minute period, a notable decrease in absorbance at 400 nm was recorded across all concentrations, validating the conversion of 4-NP to 4-AP. The calculated percentage reductions were 85.83% for 2 ppm, 95% for 10 ppm, and 99% for 15 ppm, highlighting the effectiveness of $NiFe_2O_4$/POAT in the reduction process. The results show that the catalyst does a good job of helping to change 4-NP. The higher the starting concentration, the faster the reaction goes, and within 60 minutes, almost all the 4-NP has been changed.

The data in Table 1 highlights the efficiency and operating conditions of various catalysts used for the reduction of 4-nitrophenol (4-NP), a hazardous environmental pollutant. Among them, $NiFe_2O_4$ modified with polyaniline (POAT) exhibited exceptional performance, achieving reduction efficiencies of 85%, 95%, and 99% for 2 ppm, 10 ppm, and 15 ppm concentrations, respectively, within 60 minutes. Compared to other reported catalysts, $NiFe_2O_4$/POAT demonstrates significant advantages. While catalysts like $NiFe_2O_4$/RGO and Bi_2S_3@Fe_3O_4 achieved near-complete reduction, $NiFe_2O_4$/POAT maintains consistently high efficiency across varying concentrations, highlighting its robustness and suitability for visible light-driven pollutant reduction in wastewater treatment applications. Unlike many catalysts that require $NaBH_4$ as

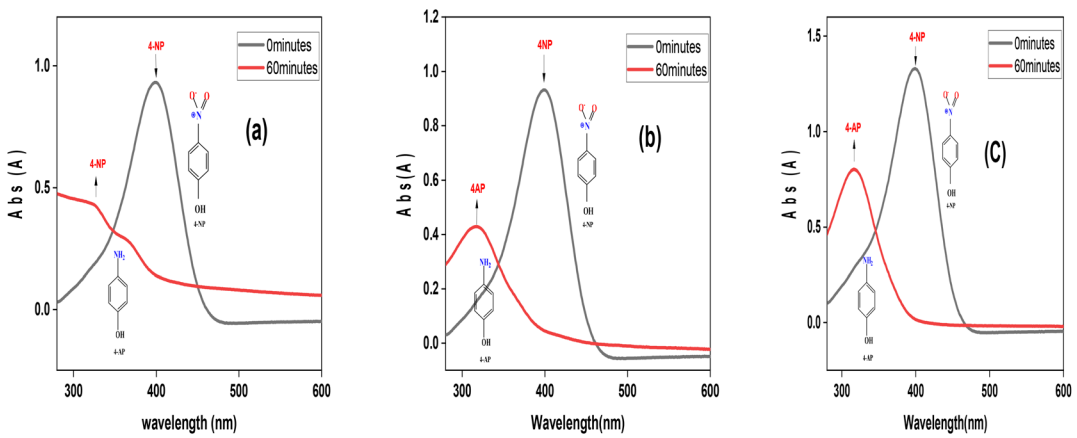

Fig. 12 The UV-Vis absorption spectra change for the reduction process of 4-NP for: (a) 2 ppm, (b) 10 ppm, and (c) 15 ppm.

Table 1 Comparison of previously reported catalysts for 4-nitrophenol reduction

Catalysts	Reduction efficiency (%)	Time (min)	Concentration	Gap energy (eV)	Reducing agent	Ref.
$NiFe_2O_4$	75	120	10 ppm	1.58	—	48
$Ni_{0.7}Cu_{0.3}Fe_2O_4$	82	120	10 ppm	1.48	—	48
$NiZnFe_2O_4$/CQDs	96	20 s	—	1.87	$NaBH_4$	33
$TiO_2/CoFe_2O_4$	95	35	10 ppm	3.2	$NaBH_4$	49
$CuFe_2O_4$	95	40 s	0.005 ppm	—	$NaBH_4$	50
$NiFe_2O_4$/RGO	100	30	0.036 M	—	$NaBH_4$	33
rGO/Cu-BDC MOF	44.67	8	0.04 mM	—	$NaBH_4$	51
$Bi_2S_3@Fe_3O_4$	98	29	0.1 mM	2.72	$NaBH_4$	52
g-C_3N_4/Bi_2S_3	60	60	0.125 mM	—	$NaBH_4$	53
Bi_2S_3 NSs	70	60	0.125 mM	—	$NaBH_4$	53
CuO/kaolinNC-1	99	12	20 ppm	—	$NaBH_4$	47
$BiFeO_3$	96	4.5	20 ppm	2.2	$NaBH_4$	54
$NiFe_2O_4$/POAT	85	60	2 ppm	1.24	—	This work
	95		10 ppm			
	99		15 ppm			

a reducing agent, this study eliminates the use of toxic and expensive chemicals, making $NiFe_2O_4$/POAT an eco-friendly and cost-effective alternative. Its alignment with green chemistry principles minimizes environmental risks and operational costs. Additionally, the lower energy band gap (1.24 eV) enhances electron transfer and catalytic activity, offering advantages over alternatives such as $NiZnFeO_4$/CQDs (1.87 eV), $TiO_2/CoFe_2O_4$ (3.2 eV), and $Bi_2S_3@Fe_3O_4$ (2.72 eV). While catalysts like $CuFe_2O_4$ achieve rapid reduction in 40 seconds, the scalability and stability of $NiFe_2O_4$/POAT over a practical 60 minute timeframe make it more suitable for industrial and real-world wastewater treatment applications. This study presents $NiFe_2O_4$/POAT as a scalable, efficient, and economically viable solution for 4-NP reduction, addressing both environmental and toxicological concerns. Its ability to function without a conventional reducing agent marks a significant step toward sustainable water treatment technologies. Overall, this work contributes to the advancement of green and innovative catalytic systems, paving the way for broader adoption in environmental remediation efforts.

Reusability of $NiFe_2O_4$/PAOT nanocomposite. The usability of $NiFe_2O_4$/PAOT nanocomposite was examined to determine whether the catalyst could be used for repeated reduction of 4-NP in successive cycles. Every cycle was carried out as described above. An external magnet bar was used to separate the catalyst from the test solution at the end of each cycle. After dipping the catalyst in 50 mL of 40 ppm NaOH for one hour, it was repeatedly cleaned with methanol and distilled water until the pH reached about 7, at which point it was dried. Sequential cycles were performed using the regenerated catalyst. eqn (3) (ref. 55) was used to determine the decreasing efficiency for % 4-NP after each cycle:

$$\text{Reduction efficiency (\%)} = ((C_0 - C_{eq})/C_0) \times 100 \quad (4)$$

From Fig. 13, it can be observed that in the first cycle, the catalyst achieves a high reduction efficiency of around 91%, indicating its initial effectiveness in reducing 4-NP. However, as the cycles progress, the reduction in efficiency significantly decreases. In the second cycle, the efficiency drops to approximately 71%, and by the third cycle, it further decreases to around 38%. By the fourth cycle, the catalyst only degrades to a minimal amount of 4-NP (~9%). The drastic decline in the fourth cycle is attributed to severe catalyst deactivation after repeated use. Several factors may contribute to this behavior: (i) partial loss of catalyst mass during recovery despite magnetic separation, (ii) surface fouling by strongly adsorbed intermediates or by-products that block active sites, (iii) structural or morphological changes during repeated reaction-regeneration cycles (including polymer detachment and reduced conductivity), and (iv) agglomeration of magnetic nanoparticles, which decreases the active surface area and dispersion in solution. While the $NiFe_2O_4$/PAOT nanocomposite shows strong catalytic activity in the initial runs, these cumulative effects limit its long-term reusability—a challenge similarly reported for ferrite–polymer composites in previous studies.[56,57]

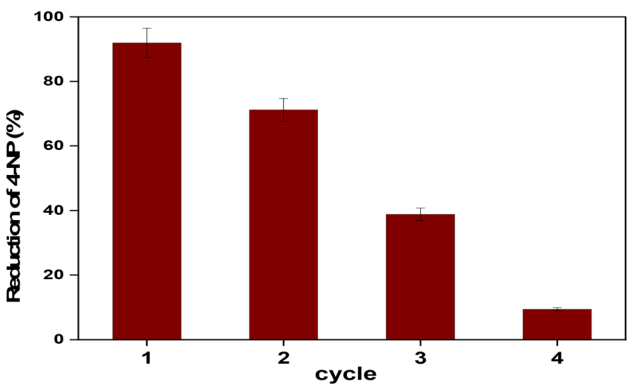

Fig. 13 Reusability of the $NiFe_2O_4$/POAT catalyst for 4-NP reduction.

Mechanism of catalytic reduction of 4-nitrophenol. The catalytic reduction of 4-nitrophenol (4-NP) to 4-aminophenol (4-AP) using $NiFe_2O_4$/POAT composite operates through an electron-driven mechanism facilitated by enhanced charge carrier dynamics.[58] $NiFe_2O_4$ represented by (Fig. 14), a ferrite

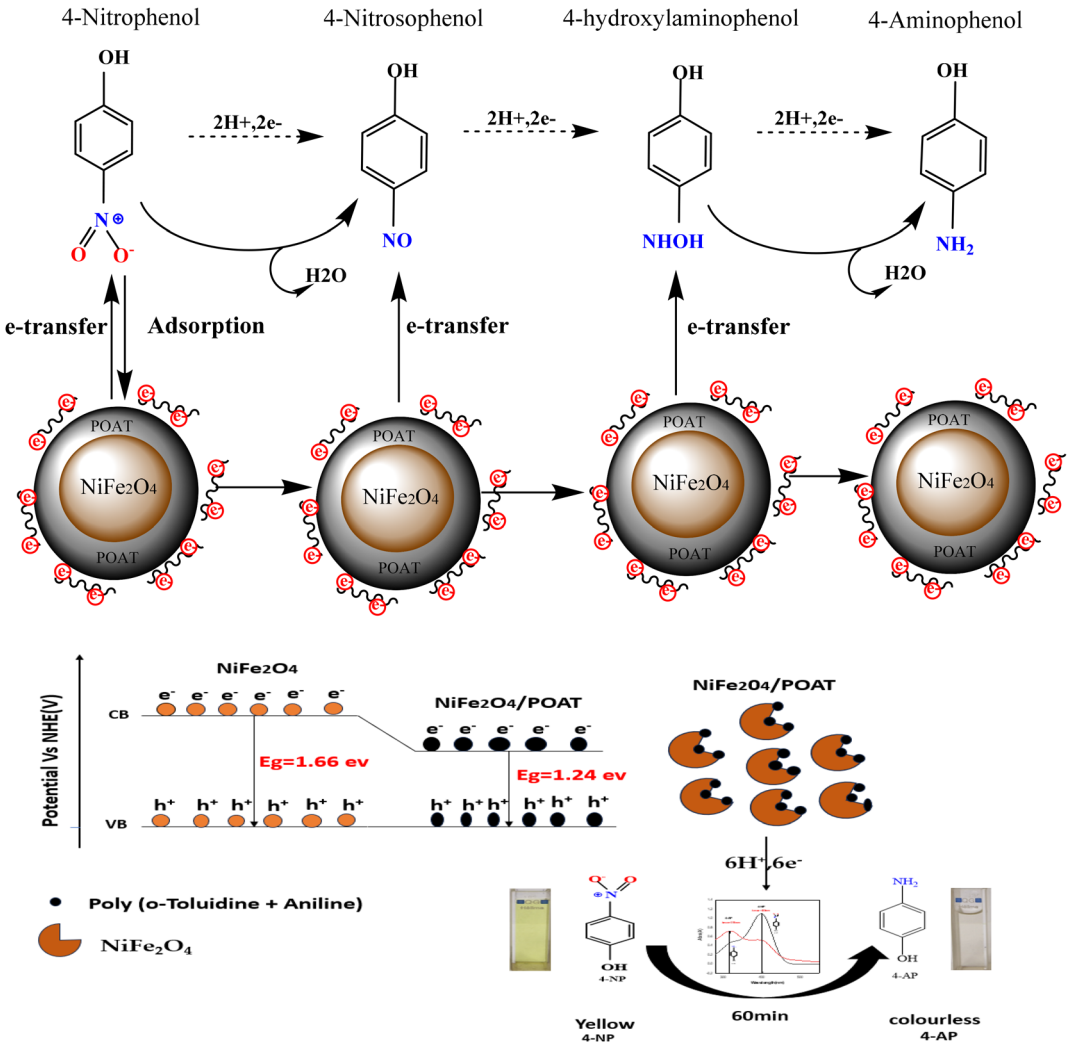

Fig. 14 Proposed mechanism of 4-nitrophenol reduction to 4-aminophenol on the catalyst surface.

material with a bandgap of 1.66 eV, absorbs visible light, generating electron–hole pairs. The incorporation of POAT into $NiFe_2O_4$ reduces the bandgap to 1.24 eV, leading to improved electron mobility and charge separation efficiency. During the reaction, electrons from the conduction band (CB) of $NiFe_2O_4$/POAT are transferred to the nitro group ($-NO_2$) of 4-NP, initiating a stepwise reduction process. The reaction proceeds through intermediate species, including nitroso (–NO) and hydroxylamine (–NHOH), ultimately yielding 4-aminophenol (4-AP) as the final product. Protons from the reaction medium combine with these electrons to complete the reduction. The composite's improved electron transport properties minimize recombination of charge carriers, ensuring a continuous supply of electrons for the reaction. The transformation is evidenced by a color change in the solution from yellow (indicating 4-NP) to colourless (indicating 4-AP). This change is further verified using UV-visible spectroscopy, which shows the disappearance of the characteristic absorption peak of 4-NP at 400 nm, and the appearance of a new peak at 318 nm. The reaction is completed within 60 min, demonstrating the superior catalytic efficiency of the $NiFe_2O_4$/POAT composite.

The 4-nitrophenol (4-NP) molecules are drawn to the surface of $NiFe_2O_4$ due to aromatic interactions: π–π stacking between the aromatic ring of 4-NP and the catalytic surface enhances adsorption. The copolymer poly(aniline-*co*-*o*-toluidine) acts as a source of electrons due to its electroactive nature. The copolymer has good electronic conductivity, which facilitates the transfer of electrons. Thanks to the oxidation/reduction cycles of the aniline and *o*-toluidine units, the polymer provides the necessary electrons for the catalytic reduction process (4-NP to 4-AP). $NiFe_2O_4$ plays the role of a semiconductor here, facilitating the migration of electrons from the copolymer to 4-nitrophenol. The Ni^{2+} and Fe^{3+} ions in the $NiFe_2O_4$ structure provide active sites that promote electron transfer and reduction reactions. The poly(aniline-*co*-*o*-toluidine) transfers electrons to the metal ions (Ni^{2+}/Fe^{3+}) on the surface of $NiFe_2O_4$. Once activated, $NiFe_2O_4$ transfers electrons to 4-nitrophenol, the band gap energy of $NiFe_2O_4$/POAT nanocomposites is low (1.24 eV) enough to excite electrons from the valence band to the conduction band. This is the main reason that facilitates the transfer of electrons from the $NiFe_2O_4$/POAT

nanocomposites to 4-nitrophenol, which is reduced to 4-aminophenol.

The conductive polymer, poly[aniline-*co*-*o*-toluidine], plays a crucial role in providing electrons for the reduction of 4-NP, $NiFe_2O_4$ facilitates electron transfer from first step: reduction of $-NO_2$ to a nitroso (–NO) intermediate[58] eqn (5), second step, reduction of –NO to an amine ($-NH_2$) eqn (6) and conversion of 4-NP to 4-aminophenol (4-AP) is represented as eqn (7).

$$-NO_2 + 2e^- + 2H^+ \rightarrow -NO + H_2O \quad (5)$$

$$-NO + 4e^- + 4H^+ \rightarrow -NH_2 + H_2O \quad (6)$$

$$C_6H_4(NO_2)OH + 6e^- + 6H^+ \rightarrow C_6H_4(NH_2)OH + 2H_2O \quad (7)$$

Conclusion

This study demonstrates the efficiency of $NiFe_2O_4$/PAOT nanocomposites in removing 4-nitrophenol (4-NP) from aqueous solutions. The catalyst demonstrated a reduction efficiency of 85% at a concentration of 2 ppm, indicating its effective performance at low pollutant levels. At concentrations of 10 ppm and 15 ppm, the reduction efficiencies were notable, achieving 95% and 99%, respectively. The consistent performance across varying concentrations highlights the adaptability of $NiFe_2O_4$/PAOT nanocomposites in effectively managing different pollutant loads. The observed bandgap energy of 1.24 eV enhances the catalyst's appeal by indicating a strong capacity for visible light absorption. This characteristic renders the nanocomposite especially appropriate for photocatalytic applications, facilitating activation by natural sunlight or artificial visible light sources, thereby significantly decreasing dependence on costly UV-based systems and enhancing energy efficiency. Leveraging visible light presents a significant advantage for environmental remediation, enhancing both the practicality and cost-effectiveness of the process. The $NiFe_2O_4$/PAOT nanocomposite exhibits high reduction efficiency and significant potential for application in wastewater treatment. The visible light activity and efficient reduction of hazardous aromatic pollutants make it a sustainable and effective solution for cleaning contaminated water sources.

Author contributions

All authors listed have made a substantial, direct, and intellectual contribution to the work and approved it for publication.

Conflicts of interest

The authors declare that the research was conducted in the absence of any commercial or financial relationships that could be constructed as a potential conflict of interest.

Data availability

Data supporting the findings of this study are available within the article.

References

1 A. Gholami, S. B. Mousavi, S. Z. Heris and M. Mohammadpourfard, Nitrate removal performance of a novel magnetic chitosan-based nanocomposite: modeling and optimization using response surface methodology, *Biomass Convers. Biorefin.*, 2024, **14**, 17481–17497.
2 R. Das, V. S. Sypu, H. K. Paumo, M. Bhaumik, V. Maharaj and A. Maity, Silver decorated magnetic nanocomposite (Fe_3O_4@PPy-MAA/Ag) as highly active catalyst towards reduction of 4-nitrophenol and toxic organic dyes, *Appl. Catal. B Environ.*, 2019, **244**, 546–558.
3 S. Z. Heris, M. Etemadi, S. B. Mousavi, M. Mohammadpourfard and B. Ramavandi, Preparation and characterizations of TiO_2/ZnO nanohybrid and its photocatalytic activity for degradation of organic dyes, *J. Photochem. Photobiol., A*, 2023, **443**, 114893.
4 X. Kong, H. Zhu, C. Chen, G. Huang and Q. Chen, Insights into the reduction of 4-nitrophenol to 4-aminophenol on catalysts, *Chem. Phys. Lett.*, 2017, **684**, 148–152.
5 Y. Shen, L. Zhang, Q. Li and X. Wang, *J. Phys. Chem. Solids*, 2022, **167**, 110783.
6 M. R. Kumar, A. S. Sekhar and S. J. Patel, *Results Chem.*, 2023, **5**, 100963.
7 S. Balgude, K. Patil, S. Moharil, M. Puranik, S. Kadam, P. Lokhande, S. Patange and P. More, *Chem. Select*, 2022, **7**, e202200221.
8 R. K. Raval and P. D. Patel, *J. Phys. Chem. Solids*, 2021, **148**, 109700.
9 S. Singh, V. K. Gupta and P. Ghosh, *RSC Adv.*, 2020, **10**, 42766–42776.
10 Z.-F. Jiang, F.-M. Tian, K.-M. Fang, Z.-G. Wang, L. Zhang, J.-J. Feng and A.-J. Wang, Atomically dispersed ternary FeCoNb active sites anchored on N-doped honeycomb-like mesoporous carbon for highly catalytic degradation of 4-nitrophenol, *J. Colloid Interface Sci.*, 2025, **677**, 718–728.
11 X. Zhang, F. Wei and S. Wang, Adsorption and catalytic degradation by $CoFe_2O_4$ coated on metal–organic framework for the removal of 4-nitrophenol and 2,4-dichlorophenol, *Sep. Purif. Technol.*, 2025, **354**, 129458.
12 S. Taghavi Fardood, F. Moradnia and T. M. Aminabhavi, Green synthesis of ZnO nanoparticles using Sargassum muticum aqueous extract and their photocatalytic degradation of methylene blue, *Environ. Pollut.*, 2024, **358**, 124534.
13 X. Liao, X. Wang, L. Zheng, Y. Hu, A. Wu and G. Li, A novel risk assessment model of urban gas pipeline network in expansions by integrating the OPA method and GraphSAGE algorithm, *Process Saf. Environ. Prot.*, 2024, **182**, 1227–1236.
14 Y. Yan, J. Miao, Z. Yang, F. X. Xiao, H. B. Yang, B. Liu and Y. Yang, Carbon nanotube catalysts: recent advances in synthesis, characterization and applications., *Chemical Society Reviews*, 2015, **44**(10), 3295–3346.
15 C. Ge, F. Shu, X. Guo, H. Jiao, D. Shi, C. Du, X. Guo, Q. Zhang, W. Wu, Y. Jin and B. Jiang, Comparison of Pd nanoparticle-decorated softwood and hardwood activated carbon in

catalytic reduction of high-concentrated industrial 4-nitrophenol, *Sep. Purif. Technol.*, 2024, **343**, 127149.
16 H. H. Shanaah, E. F. H. Alzaimoor, S. Rashdan, A. A. Abdalhafith and A. H. Kamel, Development of a novel potentiometric sensor for the determination of ketotifen fumarate in pharmaceutical formulations, *Sustainability*, 2023, **15**, 7336.
17 A. H. Kamel, H. S. M. Abd-Rabboh and A. Hefnawy, Molecularly imprinted polymer-based electrochemical sensors for monitoring the persistent organic pollutants chlorophenols, *RSC Adv.*, 2024, **14**, 20163–20181.
18 H. M. Al-Harbi, R. Kumar, M. A. Gondal and S. Al-Sayari, *Surf. Interfaces*, 2022, **33**, 102189.
19 A. Kumar, S. Sharma and V. Singh, *J. Mater. Sci.: Mater. Electron.*, 2024, **35**, 1636.
20 L. Zhao, F. Chen and M. Liu, *Inorg. Chem. Commun.*, 2024, **170**, 113170.
21 Z.-F. Jiang, F.-M. Tian, K.-M. Fang, Z.-G. Wang, L. Zhang, J.-J. Feng and A.-J. Wang, Atomically dispersed ternary FeCoNb active sites anchored on N-doped honeycomb-like mesoporous carbon for highly catalytic degradation of 4-nitrophenol, *J. Colloid Interface Sci.*, 2025, **677**, 718–728.
22 Y. Chen, H. Zhang, L. Chen, G. Fan and Y. Long, Efficient removal of 4-nitrophenol from aqueous solution using a novel magnetic biochar composite: Adsorption and catalytic degradation performance, *Sep. Purif. Technol.*, 2025, **353**, 128437.
23 A. Ammara, S. Noreen, S. Ali, S. Jamil, S. Bibi, M. J. Latif and S. R. Khan, Synthesis and characterization of chitosan-based nanocomposite for efficient removal of heavy metals from wastewater, *Polym. Bull.*, 2024, **81**, 15153–15182.
24 J. Mahmood, N. Arsalani, S. Naghash-Hamed, Z. Hanif and K. E. Geckeler, Preparation and characterization of hybrid polypyrrole nanoparticles as a conducting polymer with controllable size, *Sci. Rep.*, 2024, **14**, 11653.
25 S. S. M. Hassan, A. H. Kamel, A. A. Hassan, H. A. El-Naby, M. A. Al-Omar and A. Y. A. Sayed, *Molecules*, 2020, **25**(12), 2721.
26 A. H. Kamel, A. A. Hassan, H. H. El-Shalakany and M. A. Al-Omar, Synthesis and characterization of chitosan-based nanocomposite for efficient removal of heavy metals from wastewater, *Nanomaterials*, 2020, **10**(3), 586.
27 D. M. Dotzauer, S. Bhattacharjee, Y. Wen and M. L. Bruening, Nanoparticle-containing membranes for the catalytic reduction of nitroaromatic compounds, *Langmuir*, 2009, **25**(3), 1865–1871.
28 S. S. M. Hassan, A. H. Kamel and M. A. Fathy, A novel screen-printed potentiometric electrode with carbon nanotubes/polyaniline transducer and molecularly imprinted polymer for the determination of nalbuphine in pharmaceuticals and biological fluids, *Anal. Chim. Acta*, 2022, **1227**, 340239.
29 M. N. Ahmed, H. Khan, L. Islam, M. H. Alnasir, S. N. Ahmed, M. T. Qureshi and M. Y. Khan, Investigating nickel ferrite (NiFe2O4) nanoparticles for magnetic hyperthermia applications, *Journal of Materials and Physical Sciences*, 2023, **4**(1), 32–45.
30 Q. Qi, H. Zhang, M. Liu, S. Qi, Z. Huo, Y. Ma, Z. Zhang, Y. Lu, X. Qi, S. Han and G. Wang, Multifunctional nanoplatform for targeted cancer therapy and imaging, *Cancer Nanotechnol.*, 2023, **14**(1), 46.
31 S. Z. Heris, M. Etemadi, S. B. Mousavi, M. Mohammadpourfard and B. Ramavandi, Preparation and characterizations of TiO_2/ZnO nanohybrid and its photocatalytic activity for degradation of organic dyes, *J. Photochem. Photobiol., A*, 2023, **443**, 114893.
32 M. R. Gholipour, C. T. Dinh, F. Béland and T. O. Do, Nanostructured photocatalysts for solar hydrogen production, *Nanoscale*, 2015, **7**(18), 8187–8208.
33 S. Naghash-Hamed, N. Arsalani and E. Sharifi As, Synthesis of novel nano-structured materials for environmental applications, *Nano-Struct. Nano-Objects*, 2023, **35**, 101002.
34 S. Sambhudevan, Green Synthesis of Metal Nanoparticles for Catalytic Applications, *Chem. Pap.*, 2021, **75**, 3697–3710.
35 S. S. M. Hassan, A. H. Kamel, A. A. Hassan, A. E.-G. E. Amr, H. A. El-Naby and E. A. Elsayed, Development of Nanomaterial-Based Sensors for Environmental Monitoring, *Nanomaterials*, 2020, **10**, 254.
36 M. A. Fathy, A. H. Kamel and S. S. M. Hassan, Fabrication of Molecularly Imprinted Electrochemical Sensors for Pharmaceutical Analysis, *RSC Adv.*, 2022, **12**, 7433–7445.
37 O. Baytar, A. Ekinci, Ö. Şahin and A. Akdag, Synthesis of Novel Compounds with Potential Biological Activity, *ChemistrySelect*, 2024, **9**(8), e202304491.
38 A. G. Ramu, S. Salla, S. Chandrasekaran, P. Silambarasan, S. Gopi, S. Seo, K. Yun and D. Choi, Environmental Applications of Nanomaterials: A Review, *Environ. Pollut.*, 2021, **270**, 116063.
39 F. D. Koca and B. Şahin, Green Synthesis of $NiFe_2O_4$ Nanoparticles and Evaluation of Their Photocatalytic Activities, *Inorg. Nano-Met. Chem.*, 2024, **1**, 1–7.
40 M. Shabani, E. Saebnoori, S. A. Hassanzadeh-Tabrizi and H. R. Bakhsheshi-Rad, Synthesis and Characterization of TiO_2/ZnO Nanohybrid and Its Photocatalytic Activity for Degradation of Organic Dyes, *J. Mater. Eng. Perform.*, 2023, **32**, 2165–2182.
41 L. Sabaghzadeh, A. Tadjarodi, N. Steinfeldt and J. Strunk, Facile Synthesis of MFe_2O_4/RGO (M = Ni, Co) Nanocomposites and Their Application in the Reduction of 4-Nitrophenol, *Iran. J. Sci.*, 2024, **48**, 357–372.
42 P. Wang, D. Li, L. Wang, S. Guo, Y. Zhao, H. Shang, D. Wang and B. Zhang, Heteroatom-Doped Noble Carbon-Tailored Pd Nanoparticles for Efficient Catalytic Degradation of 4-Nitrophenol, *Chem. Eng. J.*, 2024, **495**, 153631.
43 D. M. Dotzauer, S. Bhattacharjee, Y. Wen and M. L. Bruening, Nanoparticle-Containing Membranes for the Catalytic Reduction of Nitroaromatic Compounds, *Langmuir*, 2009, **25**, 1865–1871.
44 J. Feng, L. Su, Y. Ma, C. Ren, Q. Guo and X. Chen, $CuFe_2O_4$ Magnetic Nanoparticles: A Simple and Efficient Catalyst for the Reduction of Nitrophenol, *Chem. Eng. J.*, 2013, **221**, 16–24.
45 Y. Chen, H. Zhang, L. Chen, G. Fan and Y. Long, Efficient Removal of 4-Nitrophenol from Aqueous Solution Using

a Novel Magnetic Biochar Composite: Adsorption and Catalytic Degradation Performance, *Sep. Purif. Technol.*, 2025, **353**, 128437.

46 A. O. Cardoso Juarez, E. I. Ocampo Lopez, M. K. Kesarla and N. K. R. Bogireddy, *ACS Omega*, 2024, **9**, 33335–33350.

47 Z. G. Asmare, B. A. Aragaw and M. Atlabachew, Facile Synthesis of Natural Kaolin-Based CuO Catalyst: An Efficient and Eco-Friendly Catalyst for the Reduction of 4-Nitrophenol, *ACS Omega*, 2024, **9**(49), 48014–48031.

48 P. Azhagapillai, K. Gopalsamy, I. Othman, S. Salman Ashraf, F. Banat and M. Abu Haija, Photocatalytic Reduction of 4-Nitrophenol over Eco-Friendly $Ni_xCu_xFe_2O_4$ Without an Additional Reducing Agent in Water, *Mater. Sci. Energy Technol.*, 2024, **7**, 195–204.

49 M. Khatamian, B. Divband and A. Jodaei, Synthesis and Characterization of TiO_2/ZnO Nanohybrid and Its Photocatalytic Activity for Degradation of Organic Dyes, *Mater. Chem. Phys.*, 2012, **134**, 31–37.

50 J. Feng, L. Su, Y. Ma, C. Ren, Q. Guo and X. Chen, $CuFe_2O_4$ Magnetic Nanoparticles: A Simple and Efficient Catalyst for the Reduction of Nitrophenol, *Chem. Eng. J.*, 2013, **221**, 16–24.

51 A. A. Yadav, Y. M. Hunge, S. Majumder, A.-H. I. Mourad, M. M. Islam, T. Sakurai and S.-W. Kang, Catalytic Degradation of 4-Nitrophenol in Polluted Water by Three-Dimensional Co_3O_4 Nanostructures, *J. Colloid Interface Sci.*, 2025, **677**, 161–170.

52 N. Kurnaz Yetim, N. Aslan and M. M. Koç, Synthesis and Characterization of TiO_2/ZnO Nanohybrid and Its Photocatalytic Activity for Degradation of Organic Dyes, *J. Environ. Chem. Eng.*, 2020, **8**, 104258.

53 D. Ayodhya and G. Veerabhadram, Catalytic Degradation of 4-Nitrophenol in Polluted Water by Three-Dimensional Co_3O_4 Nanostructures, *Environ. Technol.*, 2021, **42**, 826–841.

54 S. Parida, B. Sarangi, J. Nanda and B. Pany, Effect of Co^{2+} Doping on Structural, Optical, and Magnetic Properties of $NiFe_2O_4$ Nanoparticles, *Inorg. Chem. Commun.*, 2024, **170**, 113344.

55 G. B. Stambouli, B. Benguella, B. Makhoukhi, M. S. El-ouchdi and A. H. Kamel, Physicochemical properties of mesoporous acid activated materials from Lemna minor for Bezaktiv Red S-MAX dye removal, *J. Anal. Methods*, 2025, **17**, 2134–2143.

56 F. F. Alharbi, S. Gouadria, M. Abdullah, A. G. Abid, F. Mehar-un-Nisa, H. M. T. Farid and S. Aman, Development of High-Performance Alloys for Aerospace Applications, *JOM*, 2024, DOI: **10.1007/s11837-024-06964-x**.

57 T. L. Lambat, P. V. Ledade, J. K. Gunjate, V. R. Bahekar, S. H. Mahmood and S. Banerjee, Recent Developments in the Organic Synthesis Using Nano-$NiFe_2O_4$ as Reusable Catalyst: A Comprehensive Synthesis & Catalytic Reusability Protocol, *Results Chem.*, 2023, **6**, 101176.

58 T. K. Das and N. C. Das, Advances on Catalytic Reduction of 4-Nitrophenol by Nanostructured Materials as Benchmark Reaction, *Int. Nano Lett.*, 2022, **12**, 223–242.